

Symmetry Breaking Dynamics in Quantum Many-Body Systems

Hui Yu,¹ Zi-Xiang Li,^{1,2,*} and Shi-Xin Zhang^{1,†}

¹*Beijing National Laboratory for Condensed Matter Physics and Institute of Physics,
Chinese Academy of Sciences, Beijing 100910, China*

²*University of Chinese Academy of Sciences, Beijing 100049, China*

(Dated: January 24, 2025)

Entanglement asymmetry has emerged as a novel tool for characterizing symmetry breaking in quantum many-body systems. In this Letter, we investigate how symmetry is dynamically broken through the lens of entanglement asymmetry in two distinct scenarios: a non-symmetric random quantum circuit and a non-symmetric Hamiltonian quench, with a particular focus on U(1) symmetry. In the former case, the symmetry is first broken and then restored while in the latter case, symmetry remains broken in the subsystem at late times, aligning with the concept of quantum thermalization. Entanglement asymmetry growth exhibits unexpected overshooting behavior at early times in both contexts. We also consider dynamics of non-symmetric initial states under the symmetry-breaking evolution. Due to the competition of symmetry-breaking in both the initial state and Hamiltonian, the early-time entanglement asymmetry displays two qualitatively different behaviors. Furthermore, quantum Mpemba effects remain evident despite the presence of weak symmetry-breaking in both settings.

Introduction.— Symmetry breaking is a ubiquitous phenomenon across all branches of physics, ranging from high-energy physics to condensed matter physics. A well-known example is the Higgs mechanism [1] in particle physics, where the vacuum state of the universe causes different particles to acquire mass, spontaneously breaking the electroweak symmetry. This type of symmetry breaking occurs without external influences, as the symmetry is broken in the system’s ground state, a process known as spontaneous symmetry breaking. In contrast, a symmetry can also be explicitly broken when the Hamiltonian describing the system directly breaks the symmetry. How symmetry is broken dynamically in this case is an interesting fundamental question to explore.

Symmetry properties are also closely related to the concept of quantum thermalization [2–6] for generic quantum many-body systems. In general, when a closed quantum system evolves with a chaotic Hamiltonian, the reduced density matrix of a small subsystem a thermalizes to the equilibrium finite-temperature state: $\rho_a \propto e^{-\beta \hat{H}_a}$ where \hat{H}_a is the Hamiltonian of the subsystem that respects certain symmetries. In this case, symmetry is restored at later times, even if the system starts from a symmetry-broken state, since $[\hat{Q}_a, \rho_a] = 0$ where \hat{Q}_a represents the corresponding symmetry generator. However, if \hat{H}_a does not respect the symmetry, the reduced density matrix ρ_a at late times is non-commute with symmetry generator \hat{Q}_a . In this case, symmetry breaking persists to late times even if the system begins in a symmetric state.

Despite the richness of the late-time behavior, early-time dynamics have also garnered significant attention in recent years, particularly due to the novel Mpemba effect [7], which demonstrates that hot water freezes faster than cold water. Both classical and quantum

versions of the Mpemba effect have been widely explored in various systems [8–23]. Recently, quantum Mpemba effect (QME) is reported in quantum integrable systems and chaotic systems [24, 25]. U(1) symmetry is restored within a subsystem when a U(1)-asymmetric initial state evolves under the U(1)-symmetric Hamiltonian [26–36]. Notably, symmetry restoration occurs more rapidly for more asymmetric initial states. This finding was subsequently explored in various other settings [37–43] and experimentally realized on a trapped-ion quantum simulator [44].

Previous studies [24, 25] have primarily focused on characterizing symmetry restoration when an asymmetric initial state evolves under a symmetric Hamiltonian or random circuit. In contrast, this Letter examines the dynamical aspects of symmetry breaking, exploring the behavior of symmetric and asymmetric initial states under non-symmetric evolution. Besides, due to experimental limitations, symmetry evolutions are often affected by noises and defects, resulting in non-symmetric evolution as well. In such cases, can symmetry restoration still occur, or does symmetry breaking become more pronounced over time? Additionally, how does QME behave in the presence of symmetry-breaking interactions? Addressing these questions offers a more comprehensive understanding of symmetry and symmetry breaking in quantum many-body systems.

In this Letter, we investigate and compare the dynamics of symmetry breaking in a subsystem within two distinct models: a non-symmetric random circuit [45] and a non-symmetric Hamiltonian evolution, each with different symmetric and asymmetric initial states. To characterize the extent of symmetry breaking in subsystem a , we employ the metric of entanglement asymmetry (EA) [24], which has been extensively utilized as a measure of symmetry breaking in quantum

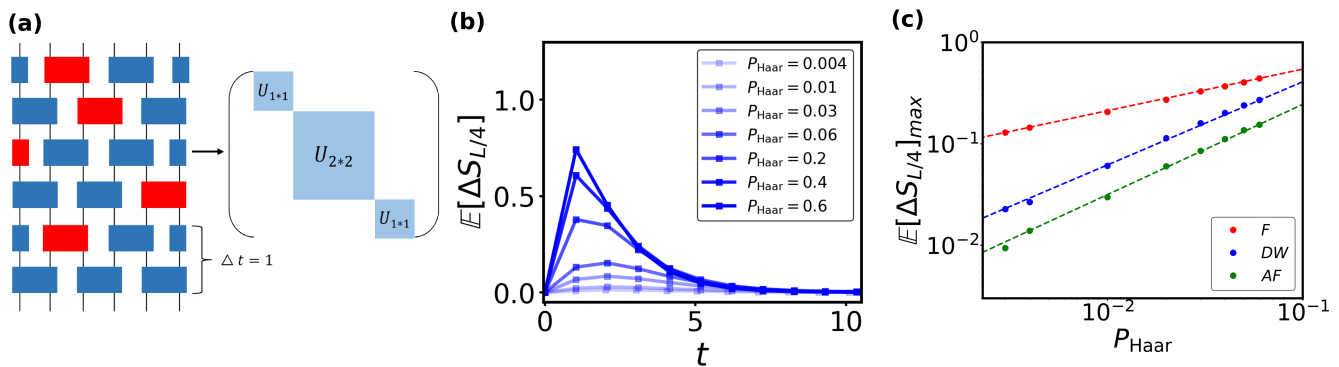


FIG. 1. (a) Schematic illustration of a non-symmetric random circuit with 6 qubits. Gates are arranged in the even-odd brick-wall pattern. The blue and red rectangles represent U(1)-symmetric and random Haar gates, respectively. The basis for the U(1)-symmetric gate are listed in the following order: $|00\rangle$, $|01\rangle$, $|10\rangle$ and $|11\rangle$. (b) The circuit-averaged EA, $\mathbb{E}[\Delta S_{L/4}]$, as a function of time with the antiferromagnetic initial state at different values of P_{Haar} . (c) The peak value, $\mathbb{E}[\Delta S_{L/4}]_{\text{max}}$, as a function of P_{Haar} . All three curves follow a power law $y = ax^b$. F: Ferromagnetic state ($a = 2.7$, $b = 0.8$); AF: Antiferromagnetic state ($a = 1.9$, $b = 0.9$).

field theories [46–48] and out-of-equilibrium many-body systems [37, 39, 49]. EA is defined as

$$\Delta S_a = S(\rho_{a,Q}) - S(\rho_a). \quad (1)$$

Here, $S(\rho_a)$ denotes the standard Von Neumann entropy of subsystem a , and $\rho_{a,Q} = \sum_{q \in \mathbb{Z}} \Pi_q \rho_a \Pi_q$ where $\hat{Q}_a = \sum_{i \in a} \sigma_i^z$ in case of U(1) symmetry of interest and Π_q is the projector onto eigenspace of \hat{Q}_a with charge q . Consequently, $\rho_{a,Q}$ is block diagonal in the eigenbasis of \hat{Q}_a . The EA satisfies two key properties: (1) $\Delta S_a \geq 0$: since the EA is defined as the relative entropy between $\rho_{a,Q}$ and ρ_a , it is non-negative by definition. (2) $\Delta S_a = 0$ if and only if $\rho_{a,Q} = \rho_a$: this implies that ρ_a is block diagonal in the eigenbasis of \hat{Q}_a . In random circuit settings, $\mathbb{E}[\Delta S_a]$ is employed as the circuit-averaged value of ΔS_a .

In the case of non-symmetric random circuits, we show that U(1) symmetry for a subsystem, with a size less than half of the total system size, can still be restored regardless of whether the initial state is U(1)-symmetric or asymmetric. As a result, EA exhibits overshooting at early times, i.e. there is a peak of EA at an early time that is much larger than the saturating EA value at late times. Additionally, QME appears at early times unless all U(1)-symmetric gates are replaced by random Haar gates, where EA dynamics are exactly the same for different U(1)-asymmetric initial states.

For a non-symmetric Hamiltonian evolution, we find that U(1) symmetry can not be restored in a subsystem. This behavior can be explained by the late-time reduced density matrix relaxing to the form $e^{-\beta \hat{H}_a}$, where \hat{H}_a explicitly includes symmetry-breaking terms. In this scenario, the EA still shows nontrivial overshooting at early times, contrasting to other symmetry-breaking

measures such as charge variance. Furthermore, early-time EA dynamics from asymmetric initial states display distinct behaviors due to the competition between two symmetry-breaking contributions related to the initial state and the system Hamiltonian. Moreover, the QME originated from symmetric evolution disappears when the strength of symmetry breaking in the evolution exceeds some thresholds.

Setup.— To characterize symmetry breaking in these systems, we consider three initial states: the ferromagnetic state $|000\dots 0\rangle$, the antiferromagnetic state $|0101\dots 1\rangle$ and the domain-wall state $|000\dots 111\rangle$, where the domain wall is positioned at the center of the chain. To incorporate the effect of symmetry breaking in the initial state, we introduce tilted ferromagnetic states, as discussed in earlier studies [24, 25]. The state is defined as

$$|\psi_i(\theta)\rangle = e^{-i\frac{\theta}{2} \sum_j \sigma_j^y} |000\dots 0\rangle \quad (2)$$

where σ_j^y is the Pauli matrix in y -direction acting on the j -th qubit, and θ is a tuning parameter that controls the strength of symmetry breaking in the initial state. When $\theta = 0$, Eq. (2) is U(1)-symmetric, resulting in a vanishing EA. As θ increases, the EA grows, reaching its maximum value when $\theta = \pi/2$. The tilted antiferromagnetic and tilted domain wall states are constructed in a similar manner.

The random circuit in Fig. 1 (a) consists of two-qubit U(1)-symmetric gates and random Haar gates, arranged in a brick-wall fashion. The exact matrix form of U(1)-symmetric gate is illustrated in Fig. 1 (a), where each block is randomly drawn from the Haar measure [50–52]. The effect of symmetry breaking depends on the density (doped probability) of random Haar gates without U(1)

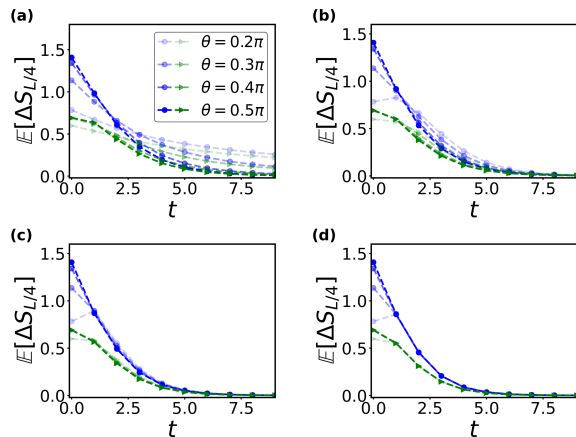


FIG. 2. The circuit-averaged EA, $\mathbb{E}[\Delta S_{L/4}]$, as a function of time for different values of P_{Haar} . Blue: U(1) EA. Green: Z_2 EA. Panels (a)-(d) correspond to different values of P_{Haar} (a) $P_{\text{Haar}} = 0$, (b) $P_{\text{Haar}} = 0.3$, (c) $P_{\text{Haar}} = 0.7$, and (d) $P_{\text{Haar}} = 1$, respectively.

symmetry, denoted as P_{Haar} . The time unit in the circuit is defined by the application of two consecutive layers of gates. The initial state $|\psi_i(\theta)\rangle$ evolves under the random unitary dynamics as the circuit progresses through successive layers of gates. $\mathbb{E}[\Delta S_a]$ is computed by averaging ΔS_a over 5000 circuit configurations.

We also investigate Hamiltonian dynamics where the state $|\psi_i(\theta)\rangle$ undergoes unitary evolution given by $e^{-iHt}|\psi_i(\theta)\rangle$, and the Hamiltonian is defined as

$$H = -\frac{1}{4} \sum_{j=1}^L \left[\sigma_j^x \sigma_{j+1}^x + \gamma \sigma_j^y \sigma_{j+1}^y + \Delta_1 \sigma_j^z \sigma_{j+1}^z \right] \quad (3)$$

$$- \Delta_2 \sum_{j=1}^L \left[\sigma_j^x \sigma_{j+2}^x + \sigma_j^y \sigma_{j+2}^y + \sigma_j^z \sigma_{j+2}^z \right].$$

Here, Δ_1 and Δ_2 are the coefficients for nearest-neighbor and next-nearest-neighbor interactions, respectively. Δ_2 introduces non-integrability, and γ controls the strength of symmetry breaking. Periodic boundary conditions are imposed in both contexts.

U(1)-Symmetric (Asymmetric) States with U(1) Non-Symmetric Random Circuit. — All numerical simulations are carried out using the TensorCircuit-NG package [53]. The circuit under investigation consists of 16 qubits. We evaluate the EA at different doping probabilities of random Haar gates, using an antiferromagnetic initial state. We observe that, at later times, all EAs approach zero, as illustrated in Fig. 1 (b). This behavior can be understood in the context of quantum thermalization and information scrambling [54–57], where the reduced density matrix of the subsystem is a fully mixed state for the random circuit cases, as long as the subsystem size does not exceed half of the total system size. Additionally, all EAs display a peak at some early time steps. For all probabilities chosen in Fig. 1 (b), all EAs reach their maximum after only a few layers of

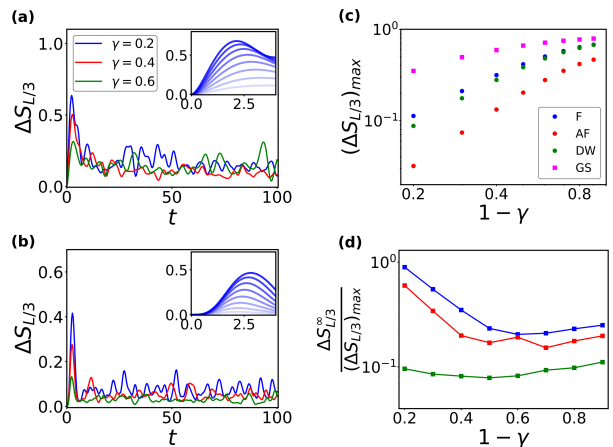


FIG. 3. EA as a function of time with (a) ferromagnetic and (b) antiferromagnetic states for different values of γ under H_{int} . The insets show the peak of EA at different values of γ . From bottom to top: $\gamma = 0.8, 0.7, 0.6, 0.5, 0.4, 0.3, 0.2, 0.1$. Panels (c) and (d) show the peak value of EA, $(\Delta S_{L/3})_{\text{max}}$, and the ratio of the late-time EA, $\Delta S_{L/3}^\infty$, to $(\Delta S_{L/3})_{\text{max}}$ as a function of $1 - \gamma$ for various initial states under H_{int} . GS represents the ground state.

unitaries. The rate of symmetry restoration also depends on the initial state. In the supplementary material (SM), we find that symmetry restoration occurs more quickly for antiferromagnetic or domain wall states than for ferromagnetic states, due to the larger Hilbert space sector of the initial states in the former cases. In Fig. 1 (c), we reveal that the peak of the circuit-averaged EA, $\mathbb{E}[\Delta S_{L/4}]_{\text{max}}$, is proportional to P_{Haar} and follows a power-law fit, with the exponent varying across different initial states.

Next, we examine the dynamics from U(1)-asymmetric initial states, i.e. a tilted ferromagnetic state, evolving under the non-symmetric random circuit. We compute the EA for both U(1) symmetry with $\hat{Q}_a = \sum_{i \in a} \sigma_i^z$ and Z_2 symmetry with $\hat{Q}_a = \prod_{i \in a} \sigma_i^z$. As depicted in Fig. 2 (a), for $P_{\text{Haar}} = 0$, we clearly notice the emergence of QME in U(1) case. Surprisingly, we also find that the QME appears in the Z_2 probe, which does not contradict previous study [25] suggesting the absence of QME in Z_2 -symmetric circuits. Even though U(1)-symmetric gates are also Z_2 symmetric, there is no off-diagonal coupling between $|00\rangle$ and $|11\rangle$, leading to different thermalization rates between two Z_2 charge sectors ($Q_a = \pm 1$), and thus resulting in QME.

As we replace a portion of U(1)-symmetric gates with random Haar gates, QME remains evident even with a finite number of random Haar gates. However, when the circuit consists entirely of random Haar gates, all charge sectors thermalize at the same rate after circuit averaging, and QME disappears. Additionally, initial information, such as the dependence on different θ -values,

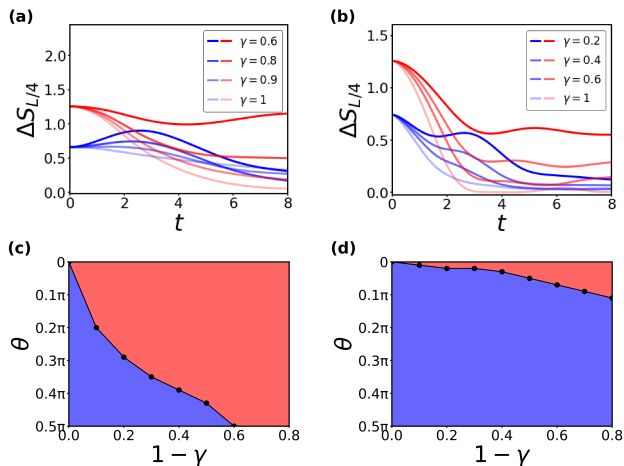


FIG. 4. EA dynamics for (a) tilted ferromagnetic states and (b) tilted antiferromagnetic states under H_{int} with different γ . The blue line corresponds to $\theta = 0.2\pi$, and the red line corresponds to $\theta = 0.5\pi$. Panels (c) and (d) show schematic 2-dimensional phase diagrams illustrating the different EA dynamics at early times on θ and $1 - \gamma$ for ferromagnetic and antiferromagnetic states, respectively. When the parameter is in the red region, EA can exceed the initial value, while in the blue region, EA firstly decreases and never grows higher than the initial value. All black dots are obtained through numerical simulation.

is erased after applying just one layer of Haar gates. Furthermore, we identify two general properties in Fig. 2. (1) For the same θ and P_{Haar} , the Z_2 EA is consistently smaller than U(1) EA. This is because the Z_2 charge sectors consist of only two sub-blocks, whereas the U(1) sectors involve smaller blocks. (2) The late-time EA for U(1)-asymmetric states approaches zero irrespective of the density of random Haar gates.

U(1)-Symmetric Initial States with U(1) Non-Symmetric Hamiltonian.— Here, we investigate the dynamics of symmetry breaking under an integrable Hamiltonian H_{int} with $\Delta_1 = 0.4$ and $\Delta_2 = 0$, and a non-integrable Hamiltonian $H_{non-int}$ with $\Delta_1 = 0.4$ and $\Delta_2 = 0.05$, with system size 12 sites. As revealed in Fig. 3 (a) and (b), we calculate EA for various Hamiltonian symmetry-breaking values γ and observe that EAs also exhibit peaks at early times that are much larger than steady values. This overshooting behavior in EA is generic for the Hamiltonian's dynamics, as long as the magnitude of Δ_1 and Δ_2 are not dominant over the XY term. Furthermore, the peak value of the EA, $(\Delta S_{L/3})_{max}$, is found to be correlated to the strength of symmetry breaking, $1 - \gamma$, for different symmetric initial states as shown in Fig. 3 (c). EA of the ground state of H_{int} follows the same trend. Notably, the peak heights nearly coincide between the ferromagnetic and domain wall states, as the early-time peak primarily depends on the local configurations of the initial state.

By analyzing Fig. 3, we identify that the late-time EA, denoted as $\Delta S_{L/3}^\infty$, oscillates and does not approach zero. This is because the reduced density matrix of subsystem a evolves towards a canonical ensemble $e^{-\beta \hat{H}_a}$, where \hat{H}_a has the same form as \hat{H} in Eq. (3), but acts solely on subsystem a . Since \hat{H}_a includes symmetry breaking terms, $[\rho_a, \hat{Q}_a] \neq 0$, leading to a non-vanishing EA at long times. In Fig. 3 (d), we calculate the ratio of $\Delta S_{L/3}^\infty$ to $(\Delta S_{L/3})_{max}$ with varying γ for different initial states. The late-time EA, $\Delta S_{L/3}^\infty$, is obtained by averaging $\Delta S_{L/3}$ over 2000 time points between $t_1 = 2000$ and $t_2 = 40000$. The results further confirm the overshooting behavior as the late-time saturating EA value is much lower than the peak value at the early time.

U(1)-Asymmetric Initial States with U(1) Non-Symmetric Hamiltonian.— Next we investigate the behavior of EA with U(1)-asymmetric initial states under H_{int} . Now, the time evolution of EA depends on both symmetry-breaking parameters, θ and γ . θ describes the symmetry breaking in the initial state and determines the initial value of EA. γ , on the other hand, serves as a measure of symmetry breaking in the Hamiltonian, which influences the evolution of the state. The interplay between these two parameters results in distinct behaviors in the time dependence of EA. This is illustrated in the schematic 2-dimensional phase diagram with varying θ and γ in Fig. 4 (c) and (d). The colors highlight the tendency in EA at early times. Blue regime indicates that $\Delta S_{L/4}(t)$ never exceeds its initial value for $t \leq 8$, while red regime corresponds to the situations where EA can grow larger than its initial value at early times. It is clearly reflected in Fig. 4 (a), the initial growth of EA at $\theta = 0.2\pi$ and $\gamma = 0.8, 0.6$ corresponds to the red region shown in the phase diagram. Two key observations are made from the phase diagram: (1) For a fixed γ , EA grows with weaker asymmetric effects (small θ) in the initial states or for a fixed θ , EA increases with stronger symmetry breaking effects (large γ) in the Hamiltonian. (2) The threshold for γ at which EA begins to rise at early times varies with different initial states. As illustrated in Fig. 4 (d), the range in which EA exceeds the initial value is very limited with an antiferromagnetic initial state within the current range of γ . In other words, the early-time behavior of EA serves as a witness to compare the symmetry-breaking strength hosting in the quantum state and the Hamiltonian. When the Hamiltonian is more asymmetric than the initial state, EA will first increase in the early time, as indicated by the red regime in the phase diagram.

In terms of another important feature in early-time dynamics, it is apparent from Fig. 4 (a) that QME emerges between $\theta = 0.2\pi$ and $\theta = 0.5\pi$ for the symmetric case $1 - \gamma = 0$. Notably, QME persists even when γ slightly deviates from one. Specifically, QME remains observable for ferromagnetic (antiferromagnetic)

initial states when $0.8 \leq \gamma \leq 1$ ($0.4 \leq \gamma \leq 1$). The robustness of QME against weak symmetry-breaking is a general feature in quantum many-body systems when the Hamiltonian is non-symmetric. We also report relevant results for non-integrable Hamiltonian $H_{non-int}$ in the SM, and the results remain qualitatively consistent with cases of H_{int} , demonstrating the universal applicability of conclusions in this Letter for Hamiltonian evolutions.

Conclusions and discussions.— In this Letter, we present a comprehensive study of subsystem symmetry breaking within two frameworks: a non-symmetric random circuit and a non-symmetric Hamiltonian evolution. Our simulation reveals that U(1) symmetry is always restored in the non-symmetric random circuit case, regardless of the initial states or the density of symmetry-breaking random Haar gates P_{Haar} . On the contrary, subsystem U(1) symmetry remains broken in the case of a U(1) non-symmetric Hamiltonian.

In addition to the late-time results, the early-time dynamics of EA shows a universal and surprising feature of overshooting. Specifically, the initial growth of EA can reach a peak significantly higher than its late-time steady value. This behavior is unexpected and is distinct from the growth of entanglement or charge variance, another measure of symmetry-breaking, where the value increases monotonically to its saturating level without any evident overshooting. Furthermore, for asymmetric initial states evolved under non-symmetric Hamiltonians, the distinct early-time dynamics of EA (increase versus decrease) allow for a direct comparison of the symmetry-breaking extent in both the state and the Hamiltonian.

There are several promising directions for further exploration. For instance, studying the dynamics of symmetry breaking in a non-unitary random circuit with mid-circuit measurements [58–74], could offer valuable insights. Additionally, examining the effect of symmetry breaking in Hamiltonians avoid thermalization such as many-body localization systems [42, 75–83] can provide a more unified picture on the understanding of symmetry-breaking dynamics.

Acknowledgement.— HY is supported by the International Young Scientist Fellowship of Institute of Physics Chinese Academy of Science (No.202407). ZXL is supported by the National Natural Science Foundation of China under the Grant No.12347107 and Grant No.12474146. SXZ is supported by a start-up grant at IOP-CAS.

* zixiangli@iphy.ac.cn

† shixinzhang@iphy.ac.cn

[1] J. Bernstein, *Reviews of modern physics* **46**, 7 (1974).
 [2] J. M. Deutsch, *Physical review A* **43**, 2046 (1991).
 [3] M. Srednicki, *Physical review E* **50**, 888 (1994).

[4] L. D’Alessio, Y. Kafri, A. Polkovnikov, and M. Rigol, *Advances in Physics* **65**, 239 (2016).
 [5] M. Rigol, V. Dunjko, and M. Olshanii, *Nature* **481**, 224 (2012).
 [6] J. M. Deutsch, *Reports on Progress in Physics* **81**, 082001 (2018).
 [7] E. B. Mpemba and D. G. Osborne, *Physics Education* **4**, 172 (1969).
 [8] Z. Lu and O. Raz, *Proceedings of the National Academy of Sciences* **114**, 5083 (2017).
 [9] A. Lasanta, F. Vega Reyes, A. Prados, and A. Santos, *Physical review letters* **119**, 148001 (2017).
 [10] A. Kumar and J. Bechhoefer, *Nature* **584**, 64 (2020).
 [11] I. Klich, O. Raz, O. Hirschberg, and M. Vucelja, *Physical Review X* **9**, 021060 (2019).
 [12] G. Teza, R. Yaacoby, and O. Raz, *Physical review letters* **131**, 017101 (2023).
 [13] J. Bechhoefer, A. Kumar, and R. Ch  trite, *Nature Reviews Physics* **3**, 534 (2021).
 [14] I. Malhotra and H. L  wen, *The Journal of Chemical Physics* **161** (2024).
 [15] A. Kumar, R. Ch  trite, and J. Bechhoefer, *Proceedings of the National Academy of Sciences* **119**, e2118484119 (2022).
 [16] S. K. Manikandan, *Physical Review Research* **3**, 043108 (2021).
 [17] A. K. Chatterjee, S. Takada, and H. Hayakawa, *Physical Review Letters* **131**, 080402 (2023).
 [18] S. Aharony Shapira, Y. Shapira, J. Markov, G. Teza, N. Akerman, O. Raz, and R. Ozeri, *Physical Review Letters* **133**, 010403 (2024).
 [19] X. Wang and J. Wang, *Physical Review Research* **6**, 033330 (2024).
 [20] A. Nava and M. Fabrizio, *Physical Review B* **100**, 125102 (2019).
 [21] F. Carollo, A. Lasanta, and I. Lesanovsky, *Physical Review Letters* **127**, 060401 (2021).
 [22] A. K. Chatterjee, S. Takada, and H. Hayakawa, *Physical Review A* **110**, 022213 (2024).
 [23] F. Ivander, N. Anto-Sztrikacs, and D. Segal, *Physical Review E* **108**, 014130 (2023).
 [24] F. Ares, S. Murciano, and P. Calabrese, *Nature Communications* **14**, 2036 (2023).
 [25] S. Liu, H.-K. Zhang, S. Yin, and S.-X. Zhang, *Physical Review Letters* **133**, 140405 (2024).
 [26] M. Fagotti, M. Collura, F. H. Essler, and P. Calabrese, *Physical Review B* **89**, 125101 (2014).
 [27] F. H. Essler and M. Fagotti, *Journal of Statistical Mechanics: Theory and Experiment* **2016**, 064002 (2016).
 [28] B. Doyon, *SciPost Physics Lecture Notes*, 018 (2020).
 [29] M. Fagotti, *Journal of Statistical Mechanics: Theory and Experiment* **2014**, P03016 (2014).
 [30] B. Bertini and M. Fagotti, *Journal of Statistical Mechanics: Theory and Experiment* **2015**, P07012 (2015).
 [31] L. Vidmar and M. Rigol, *Journal of Statistical Mechanics: Theory and Experiment* **2016**, 064007 (2016).
 [32] V. Alba, B. Bertini, M. Fagotti, L. Piroli, and P. Ruggiero, *Journal of Statistical Mechanics: Theory and Experiment* **2021**, 114004 (2021).
 [33] P. Calabrese, F. Essler, and G. Mussardo, *J. Stat. Mech* **2016**, 064001 (2016).

- [34] A. Polkovnikov, K. Sengupta, A. Silva, and M. Vengalatorre, *Mod. Phys* **83**, 5.
- [35] A. Bastianello, B. Bertini, B. Doyon, and R. Vasseur, *Journal of Statistical Mechanics: Theory and Experiment* **2022**, 014001 (2022).
- [36] F. Ares, S. Murciano, E. Vernier, and P. Calabrese, *SciPost Physics* **15**, 089 (2023).
- [37] C. Rylands, K. Klobas, F. Ares, P. Calabrese, S. Murciano, and B. Bertini, *Physical Review Letters* **133**, 010401 (2024).
- [38] S. Yamashika, F. Ares, and P. Calabrese, *Physical Review B* **110**, 085126 (2024).
- [39] B. J. Khor, D. Kürkçüoğlu, T. Hobbs, G. Perdue, and I. Klich, *Quantum* **8**, 1462 (2024).
- [40] F. Ares, S. Murciano, L. Piroli, and P. Calabrese, *Physical Review D* **110**, L061901 (2024).
- [41] S. Murciano, F. Ares, I. Klich, and P. Calabrese, *Journal of Statistical Mechanics: Theory and Experiment* **2024**, 013103 (2024).
- [42] S. Liu, H.-K. Zhang, S. Yin, S.-X. Zhang, and H. Yao, *arXiv preprint arXiv:2408.07750* (2024).
- [43] W.-X. Chang, S. Yin, S.-X. Zhang, and Z.-X. Li, *arXiv preprint arXiv:2409.06547* (2024).
- [44] L. K. Joshi, J. Franke, A. Rath, F. Ares, S. Murciano, F. Kranzl, R. Blatt, P. Zoller, B. Vermersch, P. Calabrese, *et al.*, *Physical Review Letters* **133**, 010402 (2024).
- [45] M. P. Fisher, V. Khemani, A. Nahum, and S. Vijay, *Annual Review of Condensed Matter Physics* **14**, 335 (2023).
- [46] L. Capizzi and V. Vitale, *Journal of Physics A: Mathematical and Theoretical* **57**, 45LT01 (2024).
- [47] M. Chen and H.-H. Chen, *Physical Review D* **109**, 065009 (2024).
- [48] L. Capizzi and M. Mazzoni, *Journal of High Energy Physics* **2023**, 1 (2023).
- [49] F. Ares, S. Murciano, P. Calabrese, and L. Piroli, *arXiv preprint arXiv:2501.12459* (2025).
- [50] Z. Li, H. Zheng, Y. Wang, L. Jiang, Z.-W. Liu, and J. Liu, *arXiv preprint arXiv:2309.16556* (2023).
- [51] S. N. Hearth, M. O. Flynn, A. Chandran, and C. R. Laumann, *arXiv preprint arXiv:2306.01035* (2023).
- [52] Z. Li, H. Zheng, J. Liu, L. Jiang, and Z.-W. Liu, *arXiv preprint arXiv:2309.08155* (2023).
- [53] S.-X. Zhang, J. Allcock, Z.-Q. Wan, S. Liu, J. Sun, H. Yu, X.-H. Yang, J. Qiu, Z. Ye, Y.-Q. Chen, *et al.*, *Quantum* **7**, 912 (2023).
- [54] Y.-Q. Chen, S. Liu, and S.-X. Zhang, *arXiv preprint arXiv:2405.05076* (2024).
- [55] P. Hayden and J. Preskill, *Journal of high energy physics* **2007**, 120 (2007).
- [56] Y. Sekino and L. Susskind, *Journal of High Energy Physics* **2008**, 065 (2008).
- [57] N. Lashkari, D. Stanford, M. Hastings, T. Osborne, and P. Hayden, *Journal of High Energy Physics* **2013**, 1 (2013).
- [58] P. Hosur, X.-L. Qi, D. A. Roberts, and B. Yoshida, *Journal of High Energy Physics* **2016**, 1 (2016).
- [59] B. Skinner, J. Ruhman, and A. Nahum, *Physical Review X* **9**, 031009 (2019).
- [60] S. Choi, Y. Bao, X.-L. Qi, and E. Altman, *Physical Review Letters* **125**, 030505 (2020).
- [61] Y. Li, X. Chen, and M. P. Fisher, *Physical Review B* **100**, 134306 (2019).
- [62] S.-K. Jian, C. Liu, X. Chen, B. Swingle, and P. Zhang, *Physical review letters* **127**, 140601 (2021).
- [63] T. Minato, K. Sugimoto, T. Kuwahara, and K. Saito, *Physical review letters* **128**, 010603 (2022).
- [64] S. Dhar and S. Dasgupta, *Physical Review A* **93**, 050103 (2016).
- [65] S. Vijay, *arXiv preprint arXiv:2005.03052* (2020).
- [66] Y. Bao, S. Choi, and E. Altman, *Physical Review B* **101**, 104301 (2020).
- [67] M. J. Gullans and D. A. Huse, *Physical Review X* **10**, 041020 (2020).
- [68] A. Zabalo, M. J. Gullans, J. H. Wilson, S. Gopalakrishnan, D. A. Huse, and J. Pixley, *Physical Review B* **101**, 060301 (2020).
- [69] M. Ippoliti, M. J. Gullans, S. Gopalakrishnan, D. A. Huse, and V. Khemani, *Physical Review X* **11**, 011030 (2021).
- [70] M. Szytniszewski, A. Romito, and H. Schomerus, *Physical Review B* **100**, 064204 (2019).
- [71] C.-M. Jian, Y.-Z. You, R. Vasseur, and A. W. Ludwig, *Physical Review B* **101**, 104302 (2020).
- [72] S. Liu, M.-R. Li, S.-X. Zhang, and S.-K. Jian, *Physical Review Letters* **132**, 240402 (2024).
- [73] S. Liu, M.-R. Li, S.-X. Zhang, S.-K. Jian, and H. Yao, *Physical Review B* **110**, 064323 (2024).
- [74] S. Liu, M.-R. Li, S.-X. Zhang, S.-K. Jian, and H. Yao, *Physical Review B* **107**, L201113 (2023).
- [75] F. Alet and N. Laflorencie, *Comptes Rendus Physique* **19**, 498 (2018).
- [76] D. A. Abanin, E. Altman, I. Bloch, and M. Serbyn, *Reviews of Modern Physics* **91**, 021001 (2019).
- [77] A. Pal and D. A. Huse, *Physical Review B—Condensed Matter and Materials Physics* **82**, 174411 (2010).
- [78] R. Nandkishore and D. A. Huse, *Annu. Rev. Condens. Matter Phys.* **6**, 15 (2015).
- [79] J. Z. Imbrie, V. Ros, and A. Scardicchio, *Annalen der Physik* **529**, 1600278 (2017).
- [80] E. Altman and R. Vosk, *Annu. Rev. Condens. Matter Phys.* **6**, 383 (2015).
- [81] D. A. Huse, R. Nandkishore, and V. Oganesyan, *Physical Review B* **90**, 174202 (2014).
- [82] A. Lukin, M. Rispoli, R. Schittko, M. E. Tai, A. M. Kaufman, S. Choi, V. Khemani, J. Léonard, and M. Greiner, *Science* **364**, 256 (2019).
- [83] A. Morningstar, L. Colmenarez, V. Khemani, D. J. Luitz, and D. A. Huse, *Physical Review B* **105**, 174205 (2022).

Supplemental Material for “Symmetry Breaking Dynamics in Quantum Many-Body Systems”

Contents

I. More numerical results for U(1) non-symmetric quantum circuits	7
A. Dynamics of EA with other U(1)-symmetric initial states	7
B. Dynamics of EA with tilted ferromagnetic, domain wall, and antiferromagnetic states at different P_{Haar}	7
II. More numerical results for U(1) non-symmetric Hamiltonians	9
A. Dynamics of Entanglement Asymmetry for various U(1)-symmetric initial state	9
B. Dynamics of Entanglement Entropy	9
C. Expectation values of \hat{Q} and σ_Q^2	9
D. Quantum Mempba effect in U(1) non-symmetric Hamiltonian	10
E. Phase diagrams in U(1) non-symmetric Hamiltonians	12

I. More numerical results for U(1) non-symmetric quantum circuits

A. Dynamics of EA with other U(1)-symmetric initial states

In this section, we present numerical results of the dynamics of entanglement asymmetry with different initial states, using the same setup as described in the main text. Similar to the behavior observed in Fig. 1 (b), EA for the other initial states in Fig. S1 also exhibits an initial peak, which then gradually decays to zero, indicating the restoration of U(1) symmetry. It is most apparent from the case of ferromagnetic states that a smaller density of random Haar gates results in a longer time of symmetry restoration in the subsystem. In addition, the thermalization process occurs more rapidly in domain wall and antiferromagnetic states than ferromagnetic states. This is because, in the limit of symmetry-preserving circuits, the Hilbert space accessible to the antiferromagnetic states is much larger than the ferromagnetic cases.

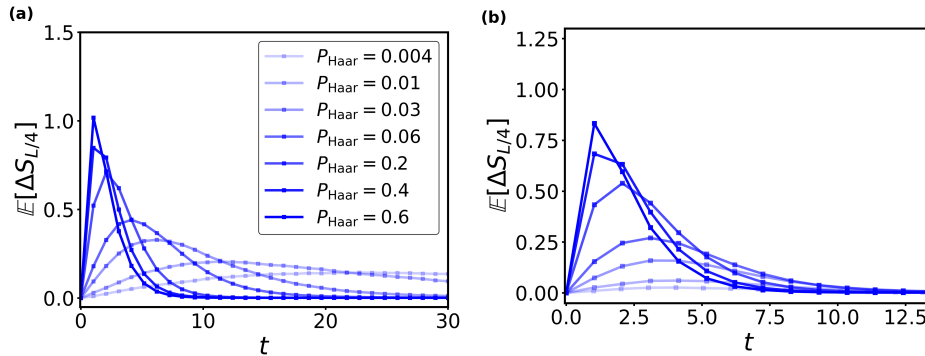


FIG. S1. The dynamics of circuit-averaged EA, $\mathbb{E}[\Delta S_{L/4}]$ for two additional initial states with $L = 16$. The varying color intensity represents different densities of random Haar gates. Left: Ferromagnetic state. Right: Domain Wall state.

B. Dynamics of EA with tilted ferromagnetic, domain wall, and antiferromagnetic states at different P_{Haar}

In addition to the P_{Haar} values used in the main text, we show the behavior of entanglement asymmetry with tilted ferromagnetic state for other P_{Haar} values in Fig. S2, and find that QME is indeed present except when the symmetry breaking reaches the maximum $P_{\text{Haar}} = 1$. This phenomenon also holds true for tilted domain wall state, as demonstrated in Fig. S3. On the contrary, as shown in Fig. S4, QME is absent for tilted antiferromagnetic states

across all values of P_{Haar} . Therefore, the emergence of QME is specific to certain initial states and is robust against the effects of random Haar gates on the circuit evolution.

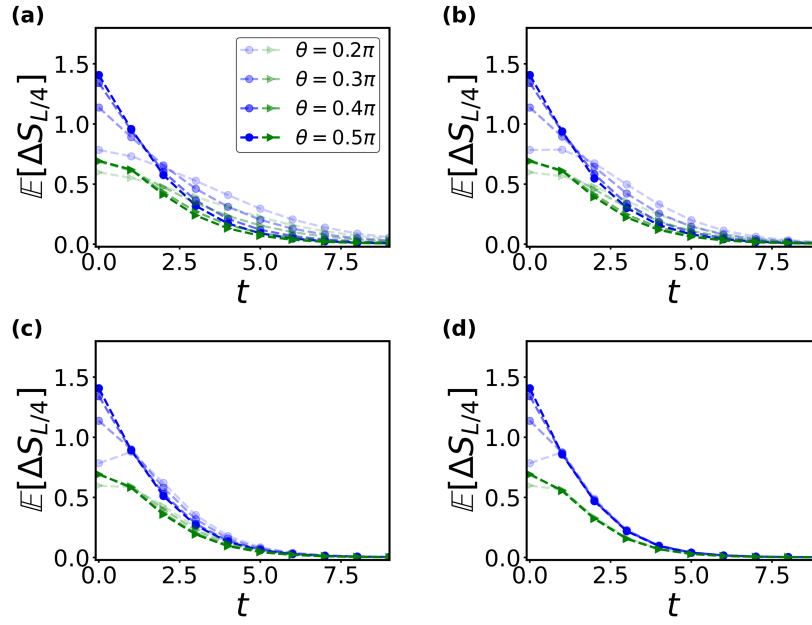


FIG. S2. The dynamics of circuit-averaged EA, $\mathbb{E}[\Delta S_{L/4}]$, for tilted ferromagnetic initial states is examined for various values of P_{Haar} with $L=16$. Blue: $U(1)$ EA. Green: Z_2 EA. Panels (a)-(d) correspond to the following values of P_{Haar} (a) $P_{\text{Haar}} = 0.1$, (b) $P_{\text{Haar}} = 0.2$, (c) $P_{\text{Haar}} = 0.5$, and (d) $P_{\text{Haar}} = 0.9$.

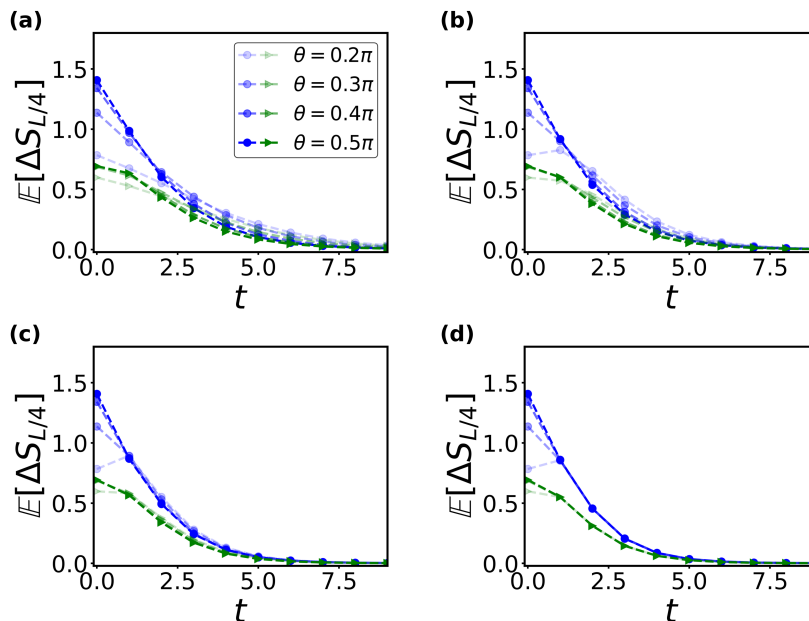


FIG. S3. The dynamics of circuit-averaged EA, $\mathbb{E}[\Delta S_{L/4}]$, for tilted domain wall initial states is examined for various values of P_{Haar} with $L=16$. Blue: $U(1)$ EA. Green: Z_2 EA. Panels (a)-(d) correspond to the following values of P_{Haar} (a) $P_{\text{Haar}} = 0$, (b) $P_{\text{Haar}} = 0.3$, (c) $P_{\text{Haar}} = 0.7$, and (d) $P_{\text{Haar}} = 1$.

II. More numerical results for $U(1)$ non-symmetric Hamiltonians

A. Dynamics of Entanglement Asymmetry for various $U(1)$ -symmetric initial state

In Fig. S5, we show the dynamics of EA across all initial states (ferromagnetic, domain wall, and antiferromagnetic) under the evolution of $H_{\text{non-int}}$. The entanglement asymmetry shows evident overshooting at early times, and the $U(1)$ symmetry remains broken in the subsystem at long times in all cases, consistent with the cases described in the main text. As shown in Fig. S6, the peak of entanglement asymmetry also correlates with the strength of symmetry breaking, $1 - \gamma$, for various initial states, including the ground state, in the case of a non-integrable Hamiltonian. Additionally, the peak value of entanglement asymmetry is significantly higher than its late-time value.

B. Dynamics of Entanglement Entropy

To better explain the behavior of entanglement asymmetry, we examine the time evolution of entanglement entropy and explore its connection to entanglement asymmetry in this section. We present both $S_{L/3}$ and $S_{L/3,Q}$ as functions of time, with their difference yielding EA, for various initial states and Hamiltonians. As shown in Fig. S7, we observe that the entanglement entropy grows linearly with time before eventually reaching a plateau. The saturation time of the entanglement entropy is always greater than the time at which the entanglement asymmetry reaches its peak. In most cases, the peak of entanglement asymmetry occurs after $S_{L/3,Q}$ reaches its first peak. This observation is reflected in Fig. S7.

C. Expectation values of \hat{Q} and σ_Q^2

The expectation value of the total spin in the z -direction as a function of time is shown in Fig. S8 for ferromagnetic states. At the start, $Q_{\text{tot}} = L = 12$ since all the spins are aligned upward. Over time, the state progressively loses memory of its initial configuration, and Q_{tot} settles into oscillations around 0. This behavior reflects the characteristics of thermalization in both non-symmetric Hamiltonians H_{int} and $H_{\text{non-int}}$. For domain wall and antiferromagnetic states, $\langle \hat{Q}_{\text{tot}}(t) \rangle = 0$ is a constant due to symmetry argument as follows.

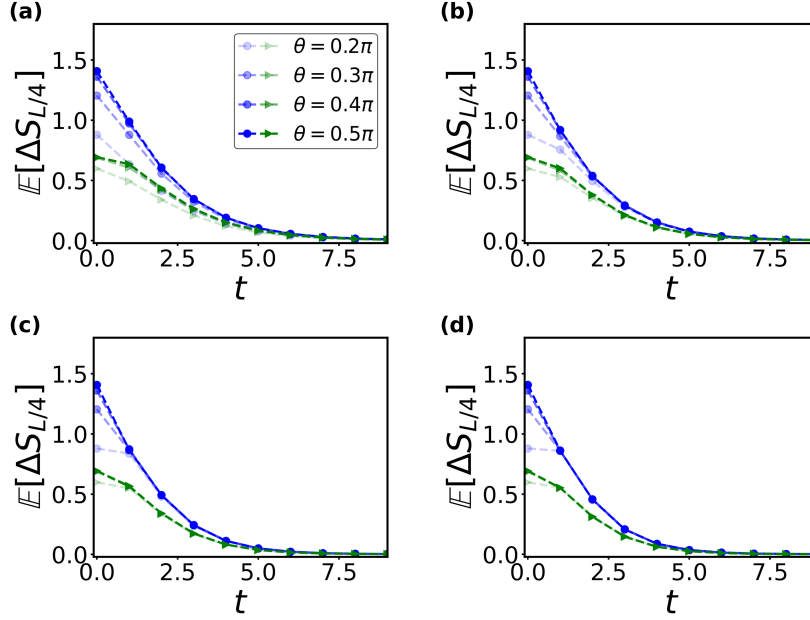


FIG. S4. The dynamics of circuit-averaged EA, $\mathbb{E}[\Delta S_{L/4}]$, for tilted antiferromagnetic initial states is examined for various values of P_{Haar} with $L=16$. Blue: U(1) EA. Green: Z_2 EA. Panels (a)-(d) correspond to the following values of P_{Haar} (a) $P_{\text{Haar}} = 0$, (b) $P_{\text{Haar}} = 0.3$, (c) $P_{\text{Haar}} = 0.7$, and (d) $P_{\text{Haar}} = 1$.

Suppose we have a transformation T :

$$T : \sigma^z \rightarrow -\sigma^z, \quad \sigma^y \rightarrow -\sigma^y \quad (\text{S1})$$

It is straightforward to verify that the Hamiltonians remain invariant under this transformation T . Thus, we have

$$\begin{aligned}
\langle \hat{Q}_{\text{tot}}(t) \rangle &= \langle \psi(t) | \hat{Q}_{\text{tot}} | \psi(t) \rangle \\
&= \langle \psi(0) | e^{iHt} \hat{Q}_{\text{tot}} e^{-iHt} | \psi(0) \rangle \\
&= \langle \psi(0) | T^\dagger T e^{iHt} T^\dagger T \hat{Q}_{\text{tot}} T^\dagger T e^{-iHt} T^\dagger T | \psi(0) \rangle \\
&= \langle \psi(0) | T^\dagger e^{iHt} (-\hat{Q}_{\text{tot}}) e^{-iHt} T | \psi(0) \rangle \\
&= \langle \psi_p(0) | e^{iHt} (-\hat{Q}_{\text{tot}}) e^{-iHt} | \psi_p(0) \rangle \\
&= -\langle \psi_p(t) | \hat{Q}_{\text{tot}} | \psi_p(t) \rangle \\
&= -\langle \psi(t) | \hat{Q}_{\text{tot}} | \psi(t) \rangle \\
&= 0
\end{aligned} \quad (\text{S2})$$

Here $|\psi_p(t)\rangle$ is related to $|\psi(t)\rangle$ by a permutation of site indices. Throughout the derivation, we use the fact that $T\hat{Q}_{\text{tot}}T^\dagger = -\hat{Q}_{\text{tot}}$. Therefore, $\langle \hat{Q}_{\text{tot}}(t) \rangle$ are strictly zero for domain wall and antiferromagnetic states.

Fig. S9 shows the time dependence of the variance of total charge operator for different initial states under H_{int} and $H_{\text{non-int}}$. Notably, the variance of the charge typically saturates later than the entanglement asymmetry. The charge variance also characterizes the U(1) symmetry breaking in the evolved state from some aspects, similar as EA explored in the main text. However, the symmetry breaking dynamical behaviors show distinct patterns in the two metrics. EA shows an evident overshooting while the charge variance directly saturates. The differences may provide further insight into the physics of symmetry breaking.

D. Quantum Mempo effect in U(1) non-symmetric Hamiltonian

When $\gamma = 1$, the emergence of QME is observed in all cases, as shown in Fig. S10. Similarly to the discussion in the main text, we find the absence of QME in the non-integrable Hamiltonian across all initial states when γ is

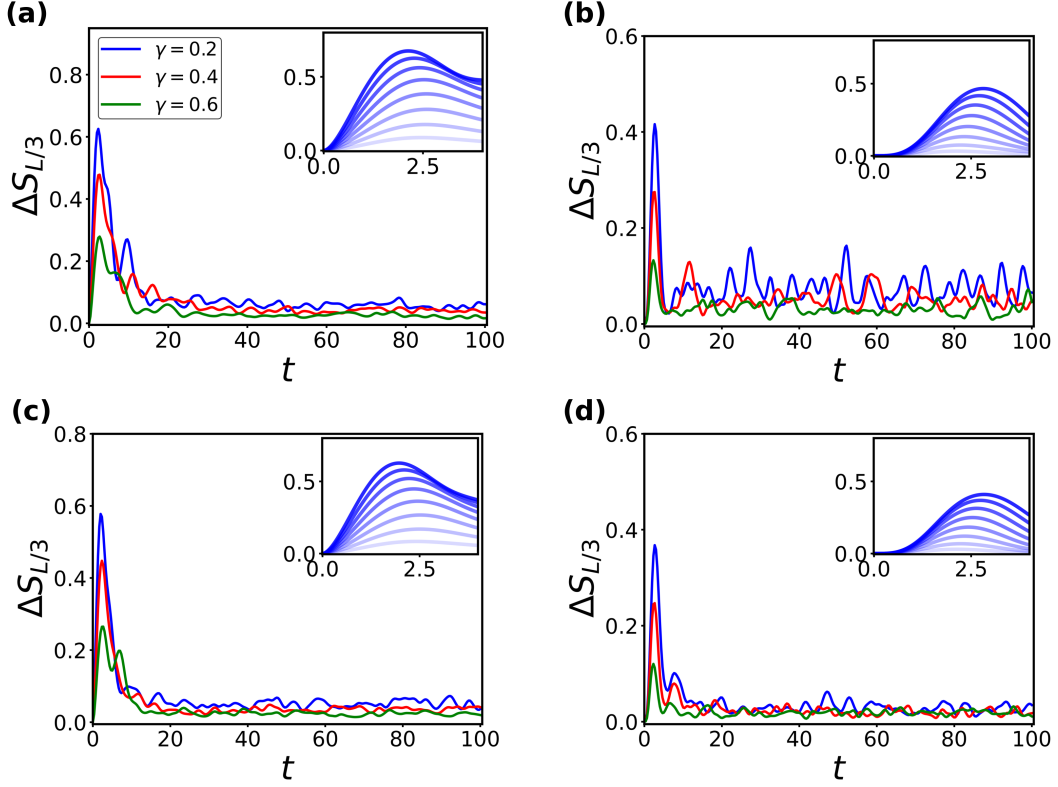


FIG. S5. EA as a function of time for various initial states and values of γ , with $L = 12$. Panels (a) are based on the H_{int} , while panels (b), (c), and (d) correspond to $H_{non-int}$. Insets zoom in on the peak of EA for different values of γ at early times, listed from bottom to top as: $\gamma = 0.8, 0.7, 0.6, 0.5, 0.4, 0.3, 0.2, 0.1$. (a),(c): Domain Wall state. (b): Ferromagnetic state. (d): Antiferromagnetic state.

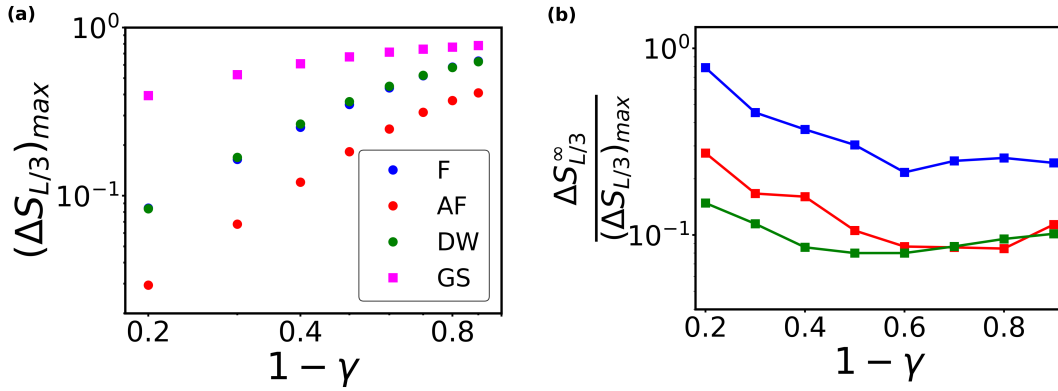


FIG. S6. Panels (a) and (b) show the peak value of EA, $(\Delta S_{L/3})_{max}$, and the ratio of the late-time EA, $\Delta S_{L/3}^{\infty}$, to $(\Delta S_{L/3})_{max}$ as a function of $1 - \gamma$ for different initial states under $H_{non-int}$. F: Ferromagnetic state; DW: Domain Wall state; AF: Antiferromagnetic state; GS: Ground State.

tuned to a certain level. Therefore, the disappearance of QME is inevitable in Hamiltonians with sufficiently strong symmetry-breaking effects.

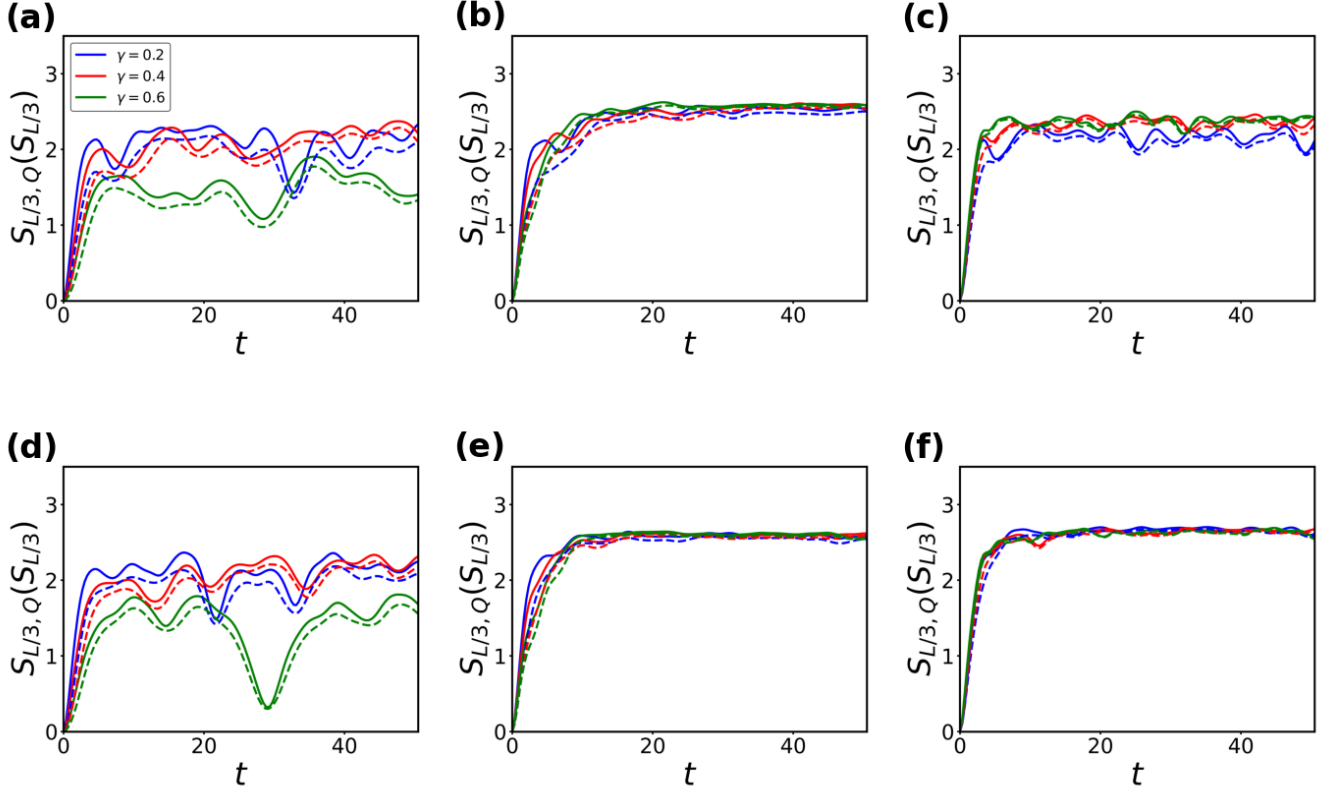


FIG. S7. Dynamics of each individual term in the expression for the entanglement asymmetry $\Delta S_{L/3}$ with $L = 12$ is shown. Solid lines represent $S_{L/3, Q}$, while dash lines correspond to the entanglement entropy $S_{L/3}$. From left to right: initial states are Ferromagnetic, Domain wall and Antiferromagnetic states, respectively. Panels (a), (b), and (c) are obtained using H_{int} , while panels (d), (e), and (f) are based on $H_{non-int}$.

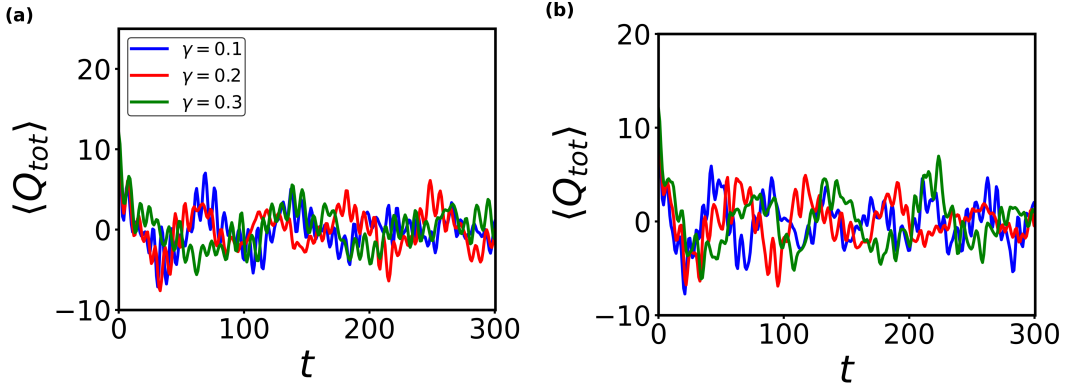


FIG. S8. The time evolution of the expectation value of the total spin in the z -direction, $\langle Q_{tot} \rangle$, is investigated for various values of γ with a ferromagnetic initial state, where $L = 12$. Here, $\hat{Q}_{tot} = \sum_{i=1}^L \sigma_i^z$. Left: H_{int} . Right: $H_{non-int}$.

E. Phase diagrams in U(1) non-symmetric Hamiltonians

As shown in Fig. S11, the phase diagrams for ferromagnetic and antiferromagnetic states obtained through $H_{non-int}$ are almost identical to those from H_{int} . A slight difference is observed in the case of the domain wall state. Since the phase boundaries are different for different initial states, a natural question arises – is the phase boundary only different in terms of θ or also different when translating θ to initial EA. In Fig. S12, we replace θ with the initial value

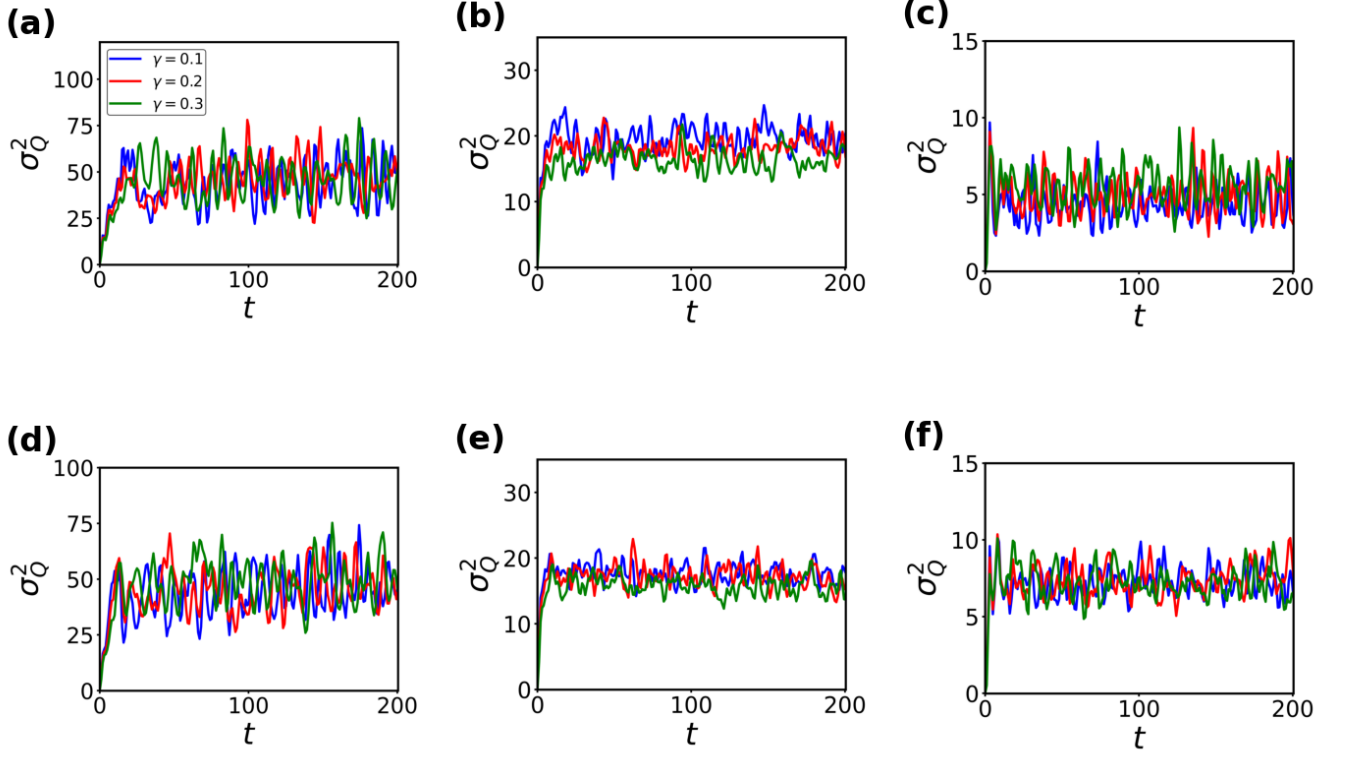


FIG. S9. The variance of Q_{tot} , σ_Q^2 , as a function of time for different values of γ with $L = 12$. Top row: H_{int} . Bottom row: $H_{non-int}$. From left to right: Ferromagnetic, Domain Wall, and Antiferromagnetic states.

of the entanglement asymmetry, $\Delta S_{L/4}^{ini}$, on the y -axis. We find that the phase boundary is still different in terms of initial EA for different types of initial states.

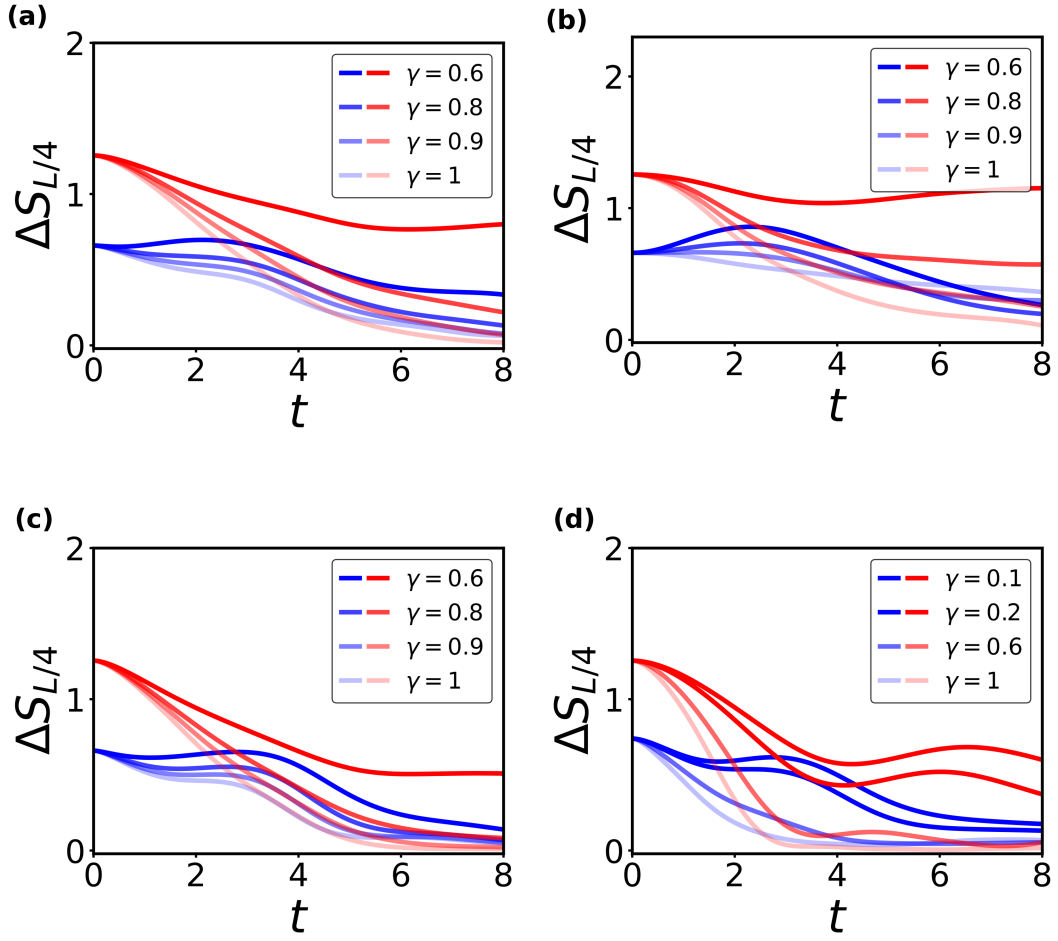


FIG. S10. EA dynamics at different values of γ with $L = 12$ are examined for (a) tilted domain wall states, (b) tilted ferromagnetic states, (c) tilted domain wall states, and (d) tilted antiferromagnetic states. Panels (b)–(d) are calculated using $H_{non-int}$, while panel (a) is based on H_{int} . Blue corresponds to $\theta = 0.2\pi$, and red corresponds to $\theta = 0.5\pi$. The increasing intensity of color reflects a stronger effect of symmetry breaking.

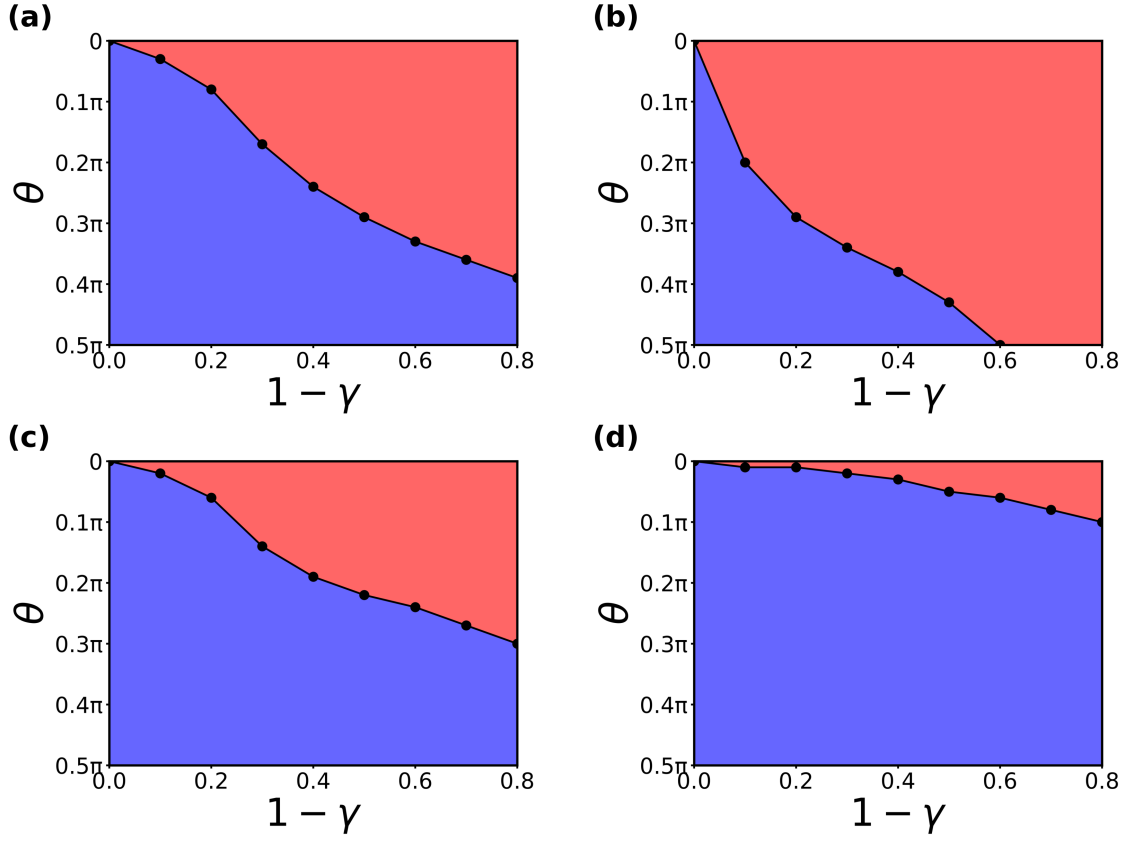


FIG. S11. Panels (a)-(d) show schematic phase diagrams depicting the dependence of EA dynamical patterns on θ and $1-\gamma$ for different initial states. (a) Domain Wall state under H_{int} , (b) Ferromagnetic state under $H_{non-int}$, (c) Domain Wall state under $H_{non-int}$, (d) Antiferromagnetic state under $H_{non-int}$. Those black dots are obtained through numerical simulation.

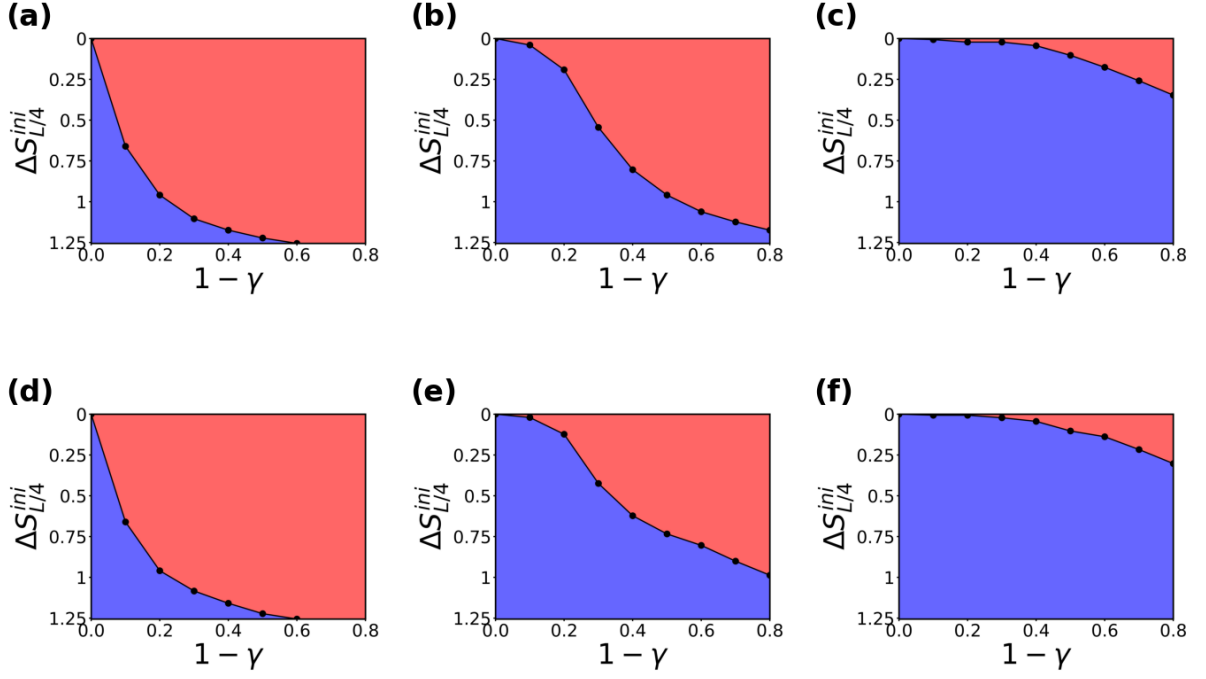


FIG. S12. Panels (a)-(f) show schematic phase diagrams depicting the dependence of EA dynamical patterns on the initial value of EA, $\Delta S_{L/4}^{ini}$ and $1 - \gamma$ for different initial states and Hamiltonians. From left to right: initial states are Ferromagnetic, Domain wall and Antiferromagnetic states, respectively. Panels (a), (b), and (c) are obtained using H_{int} , while panels (d), (e), and (f) are based on $H_{non-int}$.